DISSERTATIONS IN
FORESTRY AND
NATURAL SCIENCES

VILLE KONTTURI

Optical measurements of complex liquids

PUBLICATIONS OF THE UNIVERSITY OF EASTERN FINLAND
Dissertations in Forestry and Natural Sciences

UNIVERSITY OF
EASTERN FINLAND

VILLE KONTTURI

Optical measurements of complex liquids

Publications of the University of Eastern Finland
Dissertations in Forestry and Natural Sciences
No 50

Academic Dissertation
To be presented by permission of the Faculty of Science and Forestry for public examination in the Auditorium M102 in Metria Building at the University of Eastern Finland, Joensuu, on December, 9, 2011,
at 12 o'clock noon.

Department of Physics and Mathematics

Kopijyvä Oy
Joensuu, 2011
Editors: Prof. Pertti Pasanen,
Prof. Kai-Erik Peiponen,
Prof. Matti Vornanen

Distribution:
University of Eastern Finland Library / Sales of publications
P.O. Box 107, FI-80101 Joensuu, Finland
tel. +358-50-3058396
http://www.uef.fi/kirjasto

ISBN: 978-952-61-0586-4 (printed)
ISSNL: 1798-5668
ISSN: 1798-5668
ISBN: 978-952-61-0587-1 (pdf)
ISSNL: 1798-5668
ISSN: 1798-5676

Author's address:
University of Eastern Finland
Department of Physics and Mathematics
P.O.Box 111
80101 JOENSUU
FINLAND
email: ville.kontturi@uef.fi

Supervisors:
Professor Kai-Erik Peiponen, Ph.D., Dr. Tech
University of Eastern Finland
Department of Physics and Mathematics
P.O.Box 111
80101 JOENSUU
FINLAND
email: kai.peiponen@uef.fi

Reviewers:
Professor Fredrick W. King
University of Wisconsin-Eau Claire
Department of Chemistry,
Phillips 459,
Eau Claire,WI 54702
USA
email: fking@uwec.edu

Professor Aristide Dogariu
CREOL, The College of Optics and Photonics
University of Central Florida
P.O.Box 162700
Orlando,FL 32816
USA
email: adogariu@creol.ucf.edu

Opponent:
Docent Erik Vartiainen, Ph.D.
Lappeenranta University of Technology
Department of Mathematics and Physics
P.O.Box 20
53851 Lappeenranta
FINLAND
email: erik.vartiainen@lut.fi

ABSTRACT

This thesis is focused on novel measurement methods of the optical properties of complex liquids. Complex liquids are liquids which contain solid particles, gas bubbles or both. To obtain the optical properties of complex liquids, novel techniques are introduced to data analysis and measurement setups. Data analysis techniques are presented to obtain the colour of dry ink, quality of biofuels, number density of metallic nanoparticles, the optical properties of nanoparticles and the complex refractive index of colloidal gold. A novel measurement setup is presented for obtaining the turbidity of liquids from absorbing liquids.

Keywords: optics; optical devices; nanoparticles; spectroscopy; turbidity; biofuels
PACS Classification: 07.60.-j, 42.25.Bs, 42.25.Gy, 81.70.Fy, 82.70.-y
Universal Decimal Classification: 535.243, 535.32, 535.343.3, 535.65
Library of Congress Subject Headings: Optics; Optical instruments; Optical measurements; Liquids; Complex fluids; Spectrum analysis; Optical spectroscopy; Spectrophotometry; Colorimetry; Refractive index; Turbidity; Nanoparticles; Printing ink; Fuel; Ethanol; Colloids; Colloidal gold
Yleinen suomalainen asiasanasto: optiikka; optiset laitteet; mittaus; mittauslaitteet; nesteet; spektrianalyysi; spektroskopia; värit; sameus; nanohiukkaset; painovärit; biopolttoaineet; etanoli; kolloidit; kulta

Preface

I wish to thank my supervisor Prof. Kai-Erik Peiponen for guiding me through this thesis with an informal but encouraging way. Also I would like to thank the former head of the Department of Physics and Mathematics, Dean Prof. Timo Jääskeläinen, for the opportunity to work in our department. I express my gratitude to all my co-workers and co-authors, the research results are fruits of teamwork. Especially I want to thank Ph.D Pertti Silfsten for discussion and instructions concerning the research. Also, the thanks belong to the entire personnel, former and present, of our department. Research cannot be done without a functioning work community. I'am also indebted to my reviewers Prof. Fredrick W. King and Prof. Aristide Dogariu for their comments concerning this thesis.

Finally, I want to thank my beloved wife Minna and my dear daughters Pihla and Vilja, the most precious things in my life, for giving me the change to see what is important in life.

Joensuu 15 Oct, 2011 *Ville Kontturi*

LIST OF PUBLICATIONS

This thesis consists of the present review of the author's work in the field of optical measurements on complex liquids and the following selection of the author's publications:

I K-E Peiponen, V Kontturi, I Niskanen, M Juuti, J Räty, H Koivula and M Toivakka, "On estimation of complex refractive index and colour of dry black and cyan offset inks by a multi-function spectrophotometer," *Meas. Sci. Technol.* **19,** 115601 (2008).

II V Kontturi, S Hyvärinen, A García, R Carmona, D Yu Murzin, J-P Mikkola and K-E Peiponen, "Simultaneous detection of the absorption spectrum and refractive index ratio with a spectrophotometer: monitoring contaminants in bioethanol," *Meas. Sci. Technol.* **22,** 055803 (2011).

III Ville Kontturi, Pertti Silfsten, Jukka Räty and Kai-Erik Peiponen, "On Optical Properties of Dilute Colloidal Gold," *Plasmonics* **6,** 345–349 (2011).

IV Ville Kontturi, Pertti Silfsten, and Kai-Erik Peiponen , "Finite Frequency f-sum Rule for Assessment of Number Density of Gold Nanoparticles (AuNPs) and Kramers-Kronig Relation for Refractive Index of Colloidal Gold," *Appl. Spectrosc.* **65,** 746–749 (2011).

V Ville Kontturi, Petri Turunen, Jun Uozumi, and Kai-Erik Peiponen, "Robust sensor for turbidity measurement from light scattering and absorbing liquids," *Optics Letters* **34,** 3743–3745 (2009).

Throughout the overview, these papers will be referred to by Roman numerals. In addition, the author has contributed to publications [1–4].

AUTHOR'S CONTRIBUTION

The author conducted the colour analysis of the **Paper I**. In **Paper II** the author performed the experimental measurements and in the **Paper III** he carried out the major part of the experimental work. The author did all the calculations in **Papers II-V**. The author participated in the writing of **Papers I-V**.

Contents

1 Introduction

In society, liquids have an important role in our everyday life. The most obvious example is drinking water, the quality of which affects our lives directly [5–7]. Society and industry produces a significant amount of waste water, which needs to be decontaminated and purified before it's released back to the environment [8–11]. Another important category is liquid fuels, which are used in transportation. Nowadays a major part of transportation is still running on fossils fuels, although the amount of biofuels is rising [12, 13]. Besides transportation, the drinking-water supply and in environmental protection liquids of different kinds are handled every day in the health care sector. In many cases liquids can contain gas bubbles and solid particles, forming complex compositions, hence the measurement of liquid properties is an arduous task to perform. Although the above mentioned fields are quite different, all need information about liquids for a decision making process. Arguably the most convenient way to measure liquids is the optical method.

The basis of the optical method is that light, which the properties are known, are modulated by the material. The properties of the material can be calculated from the modulated light which is measured. In science, optical methods have been used for a long time with success and the invention of the laser [14–17] and a charge coupled device (CCD) [18] have made optical measurements relatively cheap, versatile and reliable. The decrease in the costs of the optical measurements have made it possible to utilize them in industry [19]. It is also common practice in a variety of different lines of business and in public services like environmental protection [20, 21] and health care [22–24].

In this thesis novel methods of measuring the properties of complex liquids are presented. The methods can be divided into two groups, data analysis and sensor development. In the data analysis, data from common measurement devices is used in a novel way to

obtain the properties of the samples. In the sensor development approach a new measurement setup is introduced to measure the turbidity of the sample. In chapter 2 theories related to the published papers are introduced. Chapter 2 is a brief review of the physical phenomenon lying behind the measurements rather than the full and complete description of the fundamental theories of physics. Chapter 3 discusses published results. The point of view of this chapter is to present limitations and applicability of methods in research and industry. Chapter 3 concludes with a summary which includes proposals for improving the methods in the future. The conclusion ending this thesis is presented in chapter 4.

2 On the optical properties of materials

In this chapter theories related to the interaction between light and matter are introduced. The focus of this chapter is on the theories which are related to issues studied in the published papers.

2.1 PERMITTIVITY OF MATERIALS

Interaction between light and material is mainly focused on interaction between the light and the electrons of the material. To characterize the material's response to incoming light the behaviour of the electrons plays the crucial role. Electrons in a material can be divided roughly into two groups, bound electrons and free electrons. Free electrons are able to move relatively freely in the medium. Bound electrons are unable to move in a material and are localized near to nuclei. In the interaction of light with a material, both types of electrons are contributing to the optical properties of the material. The light is electromagnetic radiation which is composed of oscillating electric and magnetic fields when light is propagating in the vacuum or the medium. In the case of optical frequencies, in general, only the electric field acts as a driving force of electrons.

2.1.1 Permittivity of bound electrons, Lorentz-model

Dielectrics are materials which do not conduct electricity when an electric field is applied across the material. At the microscopic level, it means that there are no free electrons present in the material. If the material is linear, homogenous and isotropic, then the movement of the electron has an analogy to a system of two bodies which are connected to each other with a spring. The analogy to mechanics is utilized using the Lorentz model for the permittivity. When

the applied electromagnetic field is time varying and harmonic, the displacement of the electron is written as follows [25,26]

$$x(t) = -\frac{eE_0}{m}\frac{e^{-i\omega t}}{\omega_0^2 - \omega^2 - i\Gamma\omega}, \tag{2.1}$$

where m is the mass of the electron, Γ is a damping constant, e is elementary charge, ω is the applied field circular frequency, t is time and ω_0 is the frequency of natural oscillation. The damping constant describes the attenuation of electron oscillation due to collision between the electron and the positive ion or other electrons. Separation between the electron and atomic nucleus is called the dipole moment and it is written as follows,

$$p(t) = -ex(t) = \frac{e^2}{m}\frac{E_0 e^{-i\omega t}}{\omega_0^2 - \omega^2 - i\Gamma\omega} \tag{2.2}$$

However, it is impossible to obtain dipole moment information about a single nucleus-electron pair. In the measurements, the result is the sum of all the individual electrons and it is known as polarization, which is written as follows:

$$P(t) = Np(t), \tag{2.3}$$

where N is the number density of electrons. On the other hand the polarization can be expressed as [27]

$$P(t) = (\varepsilon_0 - \varepsilon)E_0 e^{-i\omega t}, \tag{2.4}$$

where ε_0 is the permittivity of the vacuum and ε is the permittivity of the material. Material permittivity describes the material's response to an applied electric field in comparison with vacuum. Using equations (2.2), (2.4) and (2.3) we can obtain an expression for the relative permittivity as follows:

$$Re\{\varepsilon_r(\omega)\} = 1 + \frac{Ne^2}{m\varepsilon_0}\frac{\omega_0^2 - \omega^2}{(\omega_0^2 - \omega^2)^2 + \Gamma^2\omega^2} \tag{2.5}$$

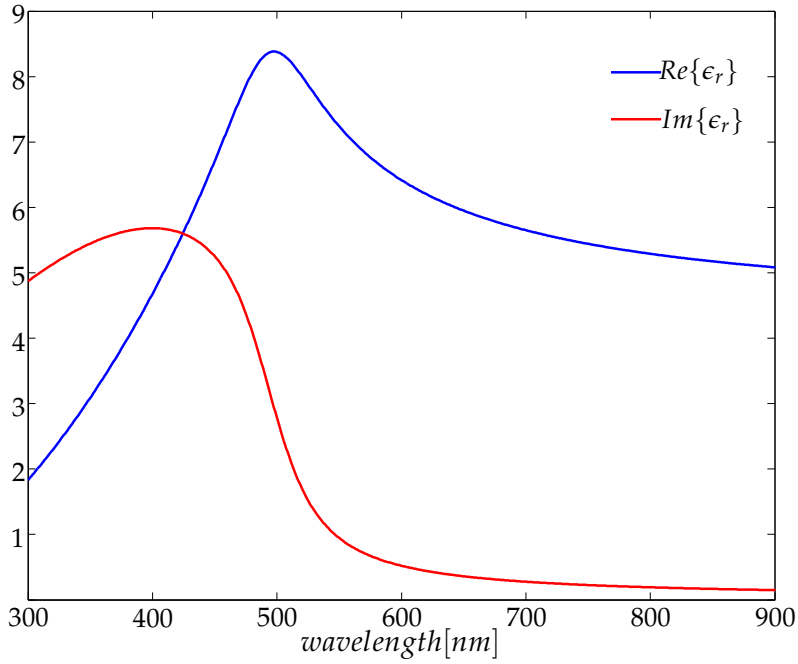

Figure 2.1: The contribution of the bound electrons to the real and imaginary parts of the relative permittivity of gold.

$$Im\{\varepsilon_r(\omega)\} = \frac{Ne^2}{m\varepsilon_0}\frac{\Gamma\omega}{(\omega_0^2-\omega^2)^2+\Gamma^2\omega^2} \tag{2.6}$$

In equations (2.5) and (2.6) $\varepsilon_r = \varepsilon/\varepsilon_0$, $\frac{Ne^2}{m\varepsilon_0} = \omega_p^2$ and ω_p is the plasma frequency which depends only on the electron density of the material. In a real medium there are several fundamental oscillator frequencies with different oscillator strengths and the permittivity of bound electrons can be described as the sum of all these oscillators. The contribution of bound electrons to the real and imaginary parts of the relative permittivity for bulk gold is shown in Fig. 2.1. Values were calculated similarly as in refs [28, 29].

2.1.2 Permittivity of free electrons, Drude-model

In conductors there are electrons that can move rather freely and hence the material can conduct an electric current. In the Drude model electrons are assumed to move against a fixed background of positive ions, forming the free electron gas. The electrons which are not bound to nuclei do not have any restoring force and hence oscillators have an undamped frequency $\omega_0 = 0$ in equation (2.1). Lack of restoring force leads equations (2.5) and (2.6) to take the following forms,

$$Re\{\varepsilon_r(\omega)\} = 1 - \frac{Ne^2}{m\varepsilon_0}\frac{1}{\omega^2 + \Gamma^2} \tag{2.7}$$

$$Im\{\varepsilon_r(\omega)\} = \frac{Ne^2}{m\varepsilon_0}\frac{\Gamma\omega}{\omega^4 + \Gamma^2\omega^2}, \tag{2.8}$$

where $\Gamma = \frac{1}{\tau}$, τ is relaxation time. The permittivity of gold arising from free electrons is shown in Fig. 2.2. In the Drude model, electrical resistance occurs when electrons collide randomly with the positive ion cores of the metal lattice. The time between collisions is the relaxation time τ and the length which electrons travel in the metal lattice between collisions is called the mean free path. Both quantities are average values of the electron behavior in the conductor. Equations (2.7) and (2.8) are valid for bulk metal but if the metal contains structures with details that are smaller than the mean free path, then the term Γ is no longer valid and needs to be modified.

Size dependent permittivity

A good example of size dependent permittivity are the spherical nanoparticles (NP). The NP's are particles with a radius of a few tens of nanometers, small enough that the model for bulk materials describes the properties of the material poorly. The small size of the particle causes the mean free path of the electrons to decrease due

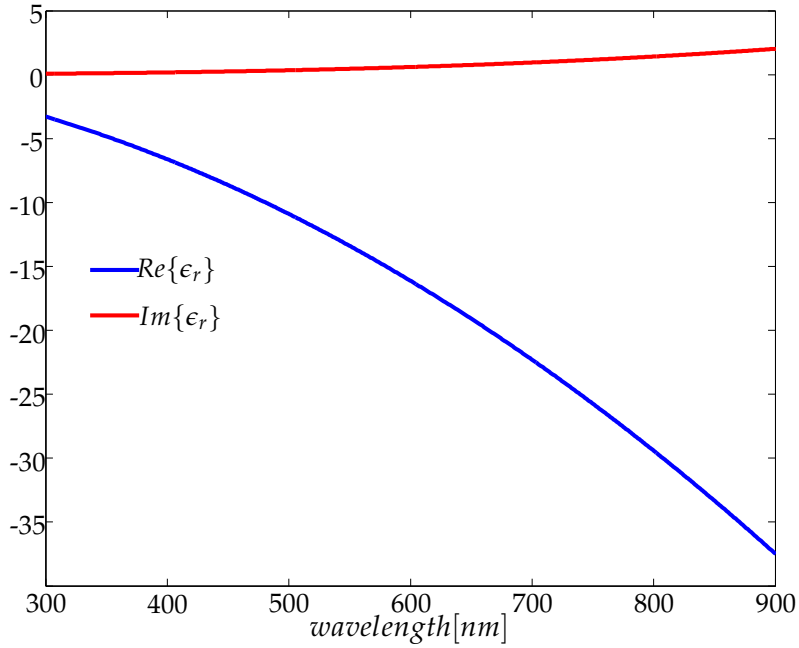

Figure 2.2: The contribution of the free electrons to the real and imaginary parts of the relative permittivity of gold.

to collisions with the boundaries of the NP [30–33]. The boundary effect can be taken into account by modification of the damping constant of the free electrons as follows [28]:

$$\Gamma(R) = \Gamma_{bulk} + \frac{Cv_F}{R}, \tag{2.9}$$

where, Γ_{bulk} is the damping constant of free electrons in the bulk material, C is the scattering constant, v_F is the electron speed at the Fermi surface and R is the radius of the particle. In equation (2.9) the scattering constant C is of the order the unity, however the exact value of this constant is not free of controversy [34]. The effect of the NP size to free electron contribution to real and imaginary part of the relative permittivity of gold is shown in Fig. 2.3 and in Fig. 2.4, respectively.

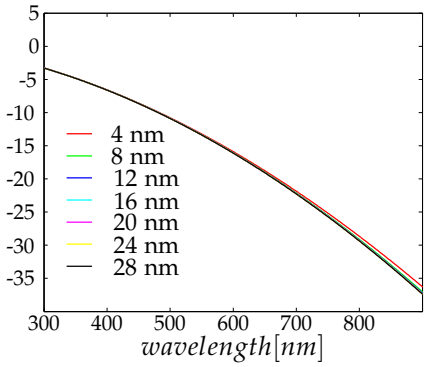

Figure 2.3: The free electron contribution to the $Re\{\varepsilon_r\}$ of gold with different particle radius.

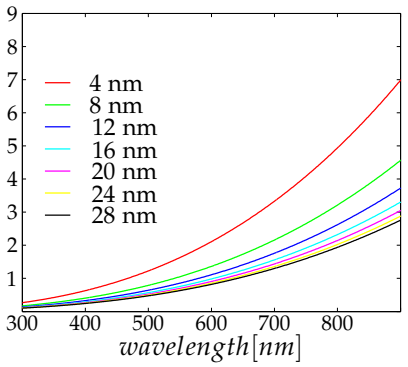

Figure 2.4: The free electron contribution to the $Im\{\varepsilon_r\}$ of gold with different particle radius.

Localized surface plasmon resonance

Another property arising from the small size of the particles, which differs from the bulk material, is the so-called localized surface plasmon resonance (LSPR). In the case of metallic NPs which are smaller than the penetration depth of the electromagnetic field, the incoming light can initiate a collective oscillation of electrons at a certain resonance frequency. The connection between the bulk materials plasma frequency and the LSPR is written as follows [35]:

$$\omega_{LSP} = \frac{\omega_p}{\sqrt{1 + 2\epsilon_m}}, \tag{2.10}$$

where ω_{LSP} is the circular frequency of the localized surface plasmon and ϵ_m is the permittivity of the medium. As can be seen from the equation (2.10) the LSPR frequency is sensitive to the host material's permittivity where metallic NPs are embedded [36]. Usually the frequency of the LSPR is approximately the frequency of the maximum absorption, however the precise frequency is dependent on the behaviour of the permittivity function ϵ_m.

2.1.3 Permittivity of complex media, Maxwell Garnett

The permittivity of materials with different substances, for example liquids with NP inclusion, cannot be modelled with the Lorentz or the Drude models. In the evaluation of a complex liquid with nano inclusion, both permittivities, the host and the inclusion, must be taken into account. Theory for the permittivity of a composite medium was introduced by J. C. Maxwell Garnett, more than a hundred years ago [37]. In the Maxwell Garnett (MG) model the assumption is that small spherical particles are distributed randomly in the host material. The equation of MG model for the effective permittivity of composite material is written as follows:

$$\frac{\varepsilon_{eff} - \varepsilon_h}{\varepsilon_{eff} + 2\varepsilon_h} = f\frac{\varepsilon_i - \varepsilon_h}{\varepsilon_i + 2\varepsilon_h}, \tag{2.11}$$

where ε_{eff} is the composite's effective permittivity, ε_h is the permittivity of the host material, ε_i is the permittivity of the inclusions and f is the volume fraction of the inclusion. The MG model works best for a dilute system ($f < 0.1$). The weakness of the MG model is that it does not take into account the real size of the particle, hence the model works only for nonscattering samples. However, the MG model could be improved to take into account the real particle size, by linking it with other theories [38, 39].

2.2 COMPLEX REFRACTIVE INDEX

The speed of light in the vacuum can be calculated from vacuum permittivity and permeability as follows:

$$c = \frac{1}{\sqrt{\varepsilon_0 \mu_0}}, \tag{2.12}$$

where μ_0 is the vacuum permeability and c is the speed of light in the vacuum. The refractive index of a material is defined as the ratio between the speed of light in the vacuum and the speed of

light in a medium:

$$n = \frac{c}{v}, \tag{2.13}$$

where v is the speed of light in the material. If the same notation is used for the speed of light in the material as in the vacuum, we get an equation for the complex refractive index as follows [40]:

$$\tilde{n} = \frac{\sqrt{\varepsilon\mu}}{\sqrt{\varepsilon_0\mu_0}}, \tag{2.14}$$

where μ is the permeability of the material. In the case of optical frequencies and nonmagnetic material the ratio $\frac{\mu}{\mu_0} \approx 1$, therefore , equation (2.14) reduces to:

$$\tilde{n} = \sqrt{\frac{\varepsilon}{\varepsilon_0}} = \sqrt{\varepsilon_r} = n + ik, \tag{2.15}$$

where n is the real refractive index and the imaginary part k is the extinction coefficient. As can be seen from Eq. (2.15) the complex refractive index is related to the relative complex permittivity of the material. In the complex refractive index, the real part of the refractive index is related to the speed of light in the material and the imaginary part describes how light is attenuated when it is propagating in the material. Relations between the real and imaginary parts of the complex refractive index and the real and imaginary parts of the relative complex permittivity are written as follows [35]

$$n = \sqrt{\frac{\sqrt{\varepsilon_{r,real}^2 + \varepsilon_{r,imag}^2} + \varepsilon_{r,real}}{2}} \tag{2.16}$$

$$k = \sqrt{\frac{\sqrt{\varepsilon_{r,real}^2 + \varepsilon_{r,imag}^2} - \varepsilon_{r,real}}{2}}, \tag{2.17}$$

where subscript *real* denotes to the real part and subscript *imag* denotes to the imaginary part of the relative permittivity.

2.2.1 Kramers–Kronig relations

The refractive index n and the extinction coefficient k are dependent on each other. The connection between the real and the imaginary parts of the complex refractive index can be expressed with the Kramers–Kronig (KK) relations [41–43] which are written as follows:

$$n(\omega') - 1 = \frac{2}{\pi} P \int_0^\infty \frac{\omega k(\omega)}{\omega^2 - \omega'^2} d\omega \tag{2.18}$$

$$k(\omega') = \frac{-2\omega'}{\pi} P \int_0^\infty \frac{n(\omega) - 1}{\omega^2 - \omega'^2} d\omega, \tag{2.19}$$

where P is the Cauchy principal value and ω' is the circular frequency where n or k is examined. The KK relations state that it is possible to obtain n if k can be measured and vice versa. A fundamental reason for the connection between n and k lies in causality [44, 45], which states that no action can happen before a stimulus. The coupling of n and k can be seen also from the permittivity equations (2.5) and (2.6) where the terms ω_0, N, Γ, which govern the permittivity response to the applied electric field, appear both in the real and imaginary parts of the relative permittivity equations.

To use equation (2.18) in order to obtain the real part of the complex refractive index one has to obtain the imaginary part of the refractive index in the spectral range $0 \rightarrow \infty$, which is practically impossible. The conversion from k to n with the aid of the KK relation with a limited spectral range leads to a result which is more likely an estimate of the dispersion of the n than the real absolute value. To overcome this measurement problem, a singly substractive Kramers–Kronig (SSKK) method was developed [46]. In the SSKK pair of n and k is known *a priori* at a certain anchor point in the measured spectral range. The utilization of known data on the anchor point leads to a faster convergence of the KK integral. The SSKK relations are written as follows:

$$n(\omega') - n(\omega'') = \frac{2(\omega'^2 - \omega''^2)}{\pi} P \int_0^\infty \frac{\omega k(\omega)}{(\omega^2 - \omega'^2)(\omega^2 - \omega''^2)} d\omega \tag{2.20}$$

$$\frac{k(\omega')}{\omega'} - \frac{k(\omega'')}{\omega''} = \frac{2(\omega'^2 - \omega''^2)}{\pi} P \int_0^\infty \frac{n(\omega) - n_\infty}{(\omega^2 - \omega'^2)(\omega^2 - \omega''^2)} d\omega, \tag{2.21}$$

where $n(\omega'')$ and $k(\omega'')$ are implicit values at an anchor point ω'' and $n_\infty = \lim_{\omega \to \infty} n(\omega)$.

2.2.2 Fresnel coefficients

Interaction of light in the interface between two different materials, with a different refractive indices, causes a part of the incoming light to reflect from the interface. Another part will be transmitted through the interface and a part will be absorbed by the material after the interface. If the interface is smooth, the amplitudes of reflected and transmitted light can be calculated using the Fresnel coefficients, which are written as follows [27].

$$R_\parallel = \left[\frac{\tilde{n}_t cos\theta_i - \tilde{n}_i cos\theta_t}{\tilde{n}_t cos\theta_i + \tilde{n}_i cos\theta_t} \right]^2 \tag{2.22}$$

$$T_\parallel = \left[\frac{2\tilde{n}_t cos\theta_i}{\tilde{n}_t cos\theta_i + \tilde{n}_i cos\theta_t} \right]^2 \tag{2.23}$$

$$R_\perp = \left[\frac{\tilde{n}_i cos\theta_i - \tilde{n}_t cos\theta_t}{\tilde{n}_i cos\theta_i + \tilde{n}_i cos\theta_t} \right]^2 \tag{2.24}$$

$$T_\perp = \left[\frac{2\tilde{n}_i cos\theta_i}{\tilde{n}_t cos\theta_t + \tilde{n}_i cos\theta_i} \right]^2, \tag{2.25}$$

where $\tilde{n}_i$ is the complex refractive index of the material where light is incoming to the interface, $\tilde{n}_t$ is the complex refractive index of the material where light penetrates after the interface and subscripts $\parallel$ and $\perp$ stand for parallel and perpendicular polarized light, respectively. The symbols θ_i and θ_t are the angles of incoming and transmitted light, respectively. Reflection and refraction of a light beam at the interface of two materials is shown in Fig. 2.5. The relation between θ_i and θ_t follows from the complex form of a Snell's law which is:

$$\tilde{n}_i sin\theta_i = \tilde{n}_t sin\theta_t \tag{2.26}$$

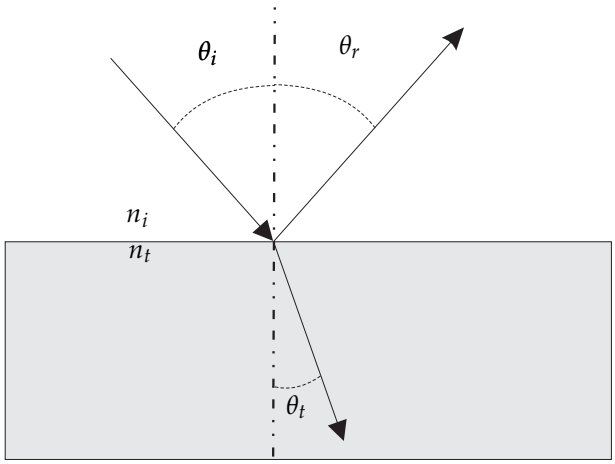

Figure 2.5: Reflection and refraction of a light beam at the interface of two different materials.

A special case of the refraction of the transmitted beam is the total internal reflection. At a certain incoming angle (known as the critical angle), the transmitted beam refracts parallel to the interface ($\theta_t = 90°$). Incoming angles higher than the critical angle cause the incoming light to reflect completely. Total internal reflection may occur only when the light comes from a higher refractive index material to a lower refractive index material ($\tilde{n}_i > \tilde{n}_t$).

Evanescent wave

In the case of the total internal reflection, the evanescent wave is induced behind the interface. Some of the incoming field will penetrate into the medium behind the interface, however the field will not be able to propagate and will attenuate at a very short distance. Attenuation of the evanescent wave in the case of total internal reflection is shown in the Fig. 2.6. The penetration depth (d_p), where the electric field is decayed to the value $E_0 e^{-1}$, where e is the Neper's number, can be expressed as follows [47]:

$$d_p = \frac{\lambda_1}{2\pi\sqrt{sin^2\theta_i - n_{21}^2}}, \tag{2.27}$$

where $\lambda_1 = \frac{\lambda}{n_1}$, $n_{21} = \frac{n_2}{n_1}$ and n_1 and n_2 are refractive indexes of different materials and $n_1 > n_2$.

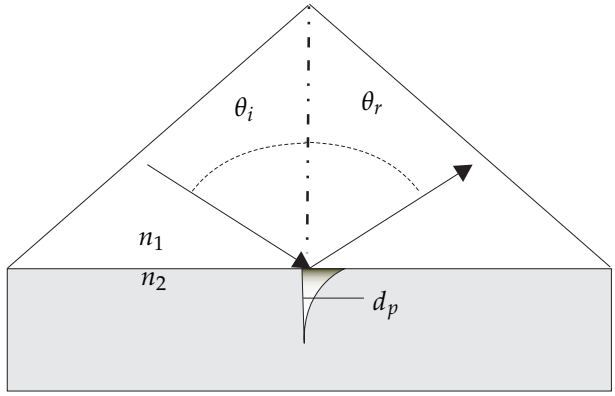

Figure 2.6: Total internal reflection and amplitude of evanescent wave

2.3 BEER-LAMBERT LAW

Attenuation of an electromagnetic wave in a homogenous medium is described by the Beer-Lambert law. The ratio between the incom-

ing and transmitted light is:

$$T = \frac{I}{I_0} = e^{-\alpha l} = e^{-\sigma N l}, \tag{2.28}$$

where I_0 is the intensity of incoming light, I is the intensity of transmitted light, α is the absorption coefficient, l is the optical path length, σ is the absorption cross section and N is the number density of the absorbers. The attenuation of an electromagnetic wave can be expressed with the absorbance as follows [26, 48]:

$$A = -ln(\frac{I}{I_0}) = \alpha l = \sigma N l \tag{2.29}$$

The connection between the imaginary part of the complex refractive index k and the absorption coefficient α is written as follows [35]:

$$\alpha = \frac{4\pi k}{\lambda} \tag{2.30}$$

The Beer-Lambert law works for clear and coloured samples and it can be used to obtain the imaginary part of the complex refractive index of the sample. However if the sample contains particles that scatter light, the attenuation of transmitted light takes the form [35]:

$$T = \frac{I}{I_0} = e^{-(\alpha_{abs}+\alpha_{sca})l}, \tag{2.31}$$

where the subscript *abs* denotes light attenuation due to absorption and subscript *sca* due to scattering. As can be seen from equation (2.31) it is impossible to separate absorption and scattering by a single measurement, because there are two independent variables and one equation to solve. Liquids containing scattering particles are called turbid liquids.

2.3.1 f-sum rule and Smakula's formula

The absorption of the electromagnetic wave in a material is a result of different absorption processes. Incoming photons can be

absorbed by phonons, conduction electrons, valence electrons or core electrons. The general absorption spectrum of a material is the sum of all of the absorbing processes mentioned above. To obtain a better picture of the material it is necessary to analyze a spectrum in the proper spectral range in order to get knowledge about the underlying process of absorption. Analyzing a spectrum in a certain spectral range is useful with a finite frequency sum rule (f-sum rule). The requirement for the utilization of the f-sum rule is that the examined absorption peak is isolated from other absorption peaks and from the background. The f-sum rule is written as follows [49]:

$$\int_{\omega_1}^{\omega_2} \omega k(\omega) d\omega \approx \frac{\pi \omega_{pi}^2}{4n}, \tag{2.32}$$

where ω_{pi} is the plasma frequency associated with the isolated absorption peak, n is the refractive index of background and ω_1 and ω_2 are the integration limits marking the isolated absorption peak.

A similar approach to the f-sum rule is the so called Smakula's formula. It can be use to calculate the number density of defect absorbers in a medium. The assumption is that there are small absorbing centers in the transparent medium and the concentration of absorbers is low. The Smakula's formula is written as follows [49–51]:

$$\rho f = S \frac{n}{(n^2+2)^2} \alpha_{eff,max} W, \tag{2.33}$$

where ρ is the density of absorbing centers, f is the oscillator strength, n is the refractive index of the host material, $\alpha_{eff,max}$ is the maximum of the absorption peak, W is the full width at half maximum of the absorption peak and S is the shape factor which is 1.57 for a Lorenzian line shape and 1.07 for a Gaussian line shape [52].

2.4 COLOUR THEORY

Colour theory exploits how the wavelength dependence of absorption, reflection or transmission of a material is observed by a human and what kind of stimulus it awakes in the brain. The colour stimulus in the brain is always an individual experience and it is related to a persons capability to see colours and his or her early experiences of colours. Because colour stimulus is based on early experiences, at least a part of the stimulus is dependent on the cultural background of the observer. To standardize the methods, results and concepts in colour theory, it is common to use spectral measurements and the so called colour-matching functions of the average observer to calculate and estimate the stimulus of the different spectral response. Colour-matching functions are experimentally measured sensitivity functions for three different light sensitive cell types in the human eye. There are two colour-matching function groups in use. One is formed from observer data from Wrigth (1928-1929) [53] and Guild (1931) [54], one from observer data from Stiles and Burch(1959) [55] and Speranskaya (1959) [56, 57]. These groups are foundations of the CIE 1931 and CIE 1964 colorimetric systems. The colour-matching functions are shown in the Fig. 2.7.

From the physical point of view the colour stimulus of the object is always a summary of three contributions: the spectral properties of illuminating light, the spectral properties of the object itself and the properties of the detector response. Three values calculated from the above-mentioned properties are called tristimulus values XYZ and equations for these are written as follows:

$$X = K \int_{\lambda} s(\lambda) S(\lambda) \bar{x}(\lambda) d\lambda \tag{2.34}$$

$$Y = K \int_{\lambda} s(\lambda) S(\lambda) \bar{y}(\lambda) d\lambda \tag{2.35}$$

$$Z = K \int_{\lambda} s(\lambda) S(\lambda) \bar{z}(\lambda) d\lambda, \tag{2.36}$$

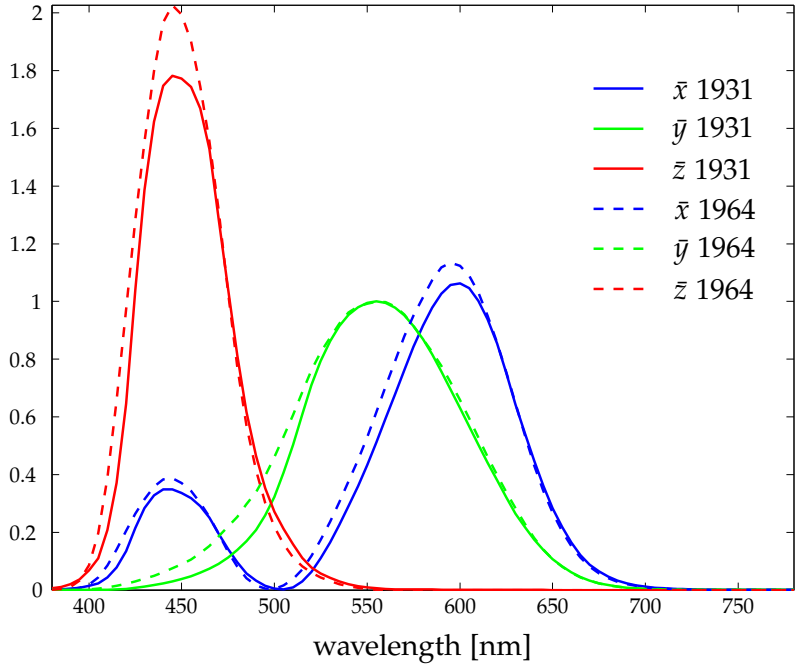

Figure 2.7: Colour-matching functions $\bar{x}$, $\bar{y}$ and $\bar{z}$ of CIE 1931 and CIE 1964 observers [58].

where K is the normalizing factor

$$K = \frac{100}{\int_\lambda S(\lambda)\bar{y}(\lambda)d\lambda}, \tag{2.37}$$

and where $s(\lambda)$ is the spectral energy distribution of the illuminant, $S(\lambda)$ the spectral response of the object, and $\bar{x}, \bar{y}$, and $\bar{z}$ are the colour-matching functions of human vision.

Tristimulus values describe colour stimulus in a rather abstract way and to describe the actual colour one can use terms like the hue and the saturation of the colour. One method for obtaining these terms from tristimulus values is to use a CIE (x,y)-chromaticity diagram.

2.4.1 CIE (x,y)-chromaticity diagram

The use of the chromaticity diagram reduces the effect of the brightness from the colour and hence the full description of the colour cannot be retrieved from the diagram. However, the diagram is a useful tool for obtaining the hue and the saturation of the colour. The connection between tristimulus values X,Y,Z and chromaticity coordinates is written as follows:

$$x = \frac{X}{X+Y+Z} \tag{2.38}$$

$$y = \frac{Y}{X+Y+Z}, \tag{2.39}$$

where x and y are chromaticity values. In the chromaticity diagram, shown in the Fig. 2.8, the outer boundary is the spectral locus composed of monochromatic light from the band of 380-700 nm. Wavelengths 380 nm and 700 nm are connected to each other with the so called purple line and there are no monochromatic counter parts for colors in the purple line. If two or more points are chosen from the chromaticity diagram, all colours which lie in the line between the points or in the area limited by chosen points can be produced by changing the ratio of colours in chosen points. The area which is limited by chosen points is called the gamut. In the center area in the chromaticity diagram is the neutral point, which represents the colour stimuli of the illuminating light source.

In the CIE (x,y)-chromaticity diagram the colour of the object can be expressed as the dominant wavelength which corresponds to the hue and the excitation purity which corresponds to the saturation of the colour. The dominant wavelength, w_d in the Fig. 2.8 is found where the line drawn from the neutral point, through the objects chromaticity coordinates and spectral locus intersects. If the intersect is found in the purple line, then the line is extended in an opposite direction so that the monochromatic wavelength can be

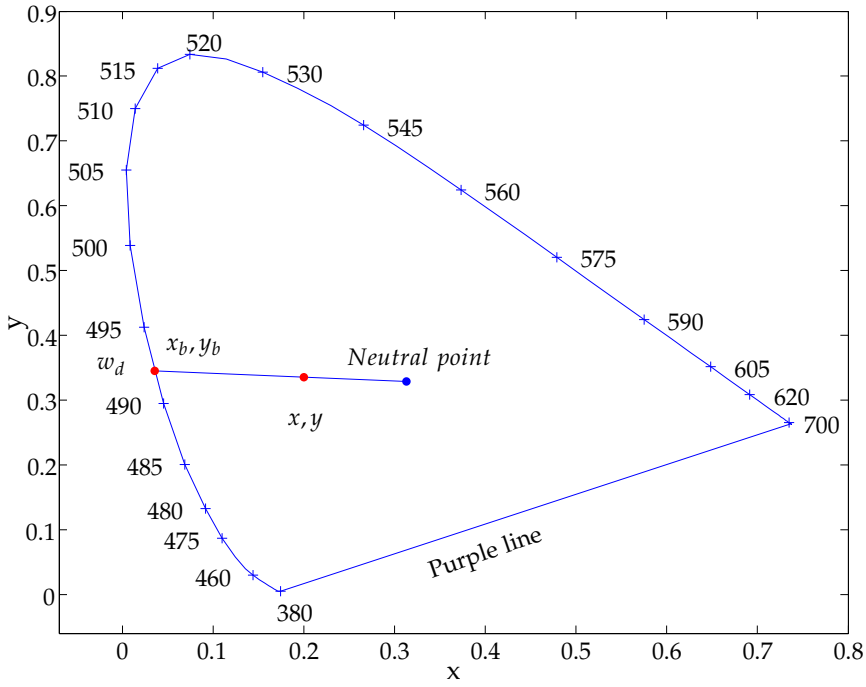

Figure 2.8: CIE (x,y)-chromaticity diagram.

obtained from the spectral locus. The negative values of the dominant wavelength denotes that the hue lies in the direction of the purple line [59]. The excitation purity can be expressed as follows:

$$p_e = \sqrt{\frac{(x - x_{NP})^2 + (y - y_{NP})^2}{(x_b - x_{NP})^2 + (y_b - y_{NP})^2}}, \tag{2.40}$$

where p_e is the excitation purity, x and y are the chromaticity values of the colour, x_{NP} and y_{NP} are the chromaticity values of neutral point, and x_b and y_b are the chromaticity values of the dominant wavelength.

3 Measurement results

In this chapter measurement results are discussed and some new results are introduced. The chapter is divided into sections by measured samples. Each section considers different measured samples and discussion about the results and boundary conditions. The chapter concludes with a future outlook, where some possible themes for research related to this thesis are introduced.

3.1 INK

Printed information applies to a very large number of people, even nowadays when digital information is making inroads into consumer products with giant leaps. The main concern of the printed product is the visual quality of the end product. The quality of printed products consists of the quality of the printing process, paper and printing ink. A printing ink can be described as the mixture of colorant, vehicle, additive and carrier substances. The vehicle ensures that ink remains on the paper, additive affects the printability of ink, a carrier substance works as transport for colorant and the colorant defines the colour of the ink [60]. To produce very pure colors the colorant should have a sharp absorption peak and thus the absorption should cut off very quickly outside of the peak. Even if the complex refractive index is not a primary quantity in the paper and printing industry, knowledge of the ink's optical properties play a crucial role in the development of new printing inks and different products with different prints.

3.1.1 Ink samples

In **Paper I** cyan (Premoterm 2000) and black (Flint Schmidt) heatset offset inks were used. The inks were spread on the measurement prism with densities of 3.6 $\frac{g}{m^2}$ for black and 14.7 $\frac{g}{m^2}$ for cyan ink. After spreading, samples were dried in the laboratory oven at a

temperature of 130°C for about one hour. The procedure made samples surface flat and optically thick.

3.1.2 Colour of the ink

In **Paper I** we measured the complex refractive index of dry black and cyan offset inks with a multifunction spectrophotometer (MFS) [61] and calculated the hue and saturation of scattered light. As can be seen from the Fig. 3.1 the intensity of scattered light is different for s- and p-polarized light for both samples. In **Paper I** the average of different polarizations of scattered light were used to obtain the colour of the unpolarized light. The colour of the s- and p- polarized light was obtained in a similar manner as described in section 2.4 and is presented in the Table 3.1.

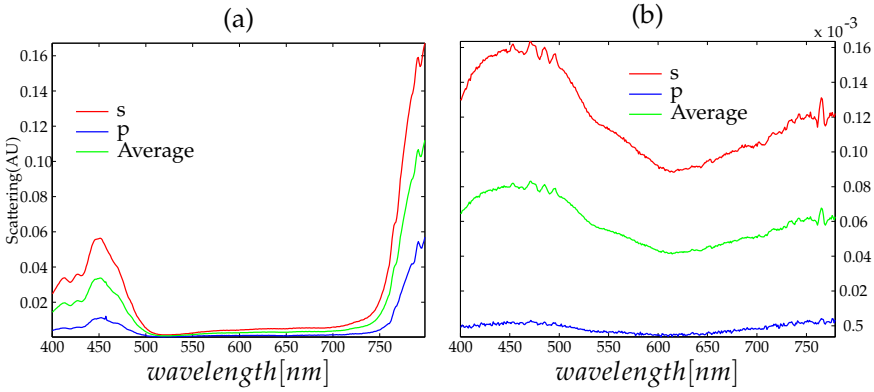

Figure 3.1: The spectra of scattered light of s- and p-polarized and average of s- and p-polarized light from (a)cyan and (b)black ink sample.

As can be seen from Table 3.1 s- and p-polarized light produce colors with slightly different dominant wavelength and excitation purity. The average of the s- and p-polarizations and s-polarized light produces almost identical x- and y-values, the difference lies in the third decimal, but the difference can be seen in the dominant wavelength and the excitation purity. The difference arises from different coupling efficiencies of the evanescent wave for different polarizations.

Table 3.1: Chromaticity values x and y, dominant wavelength and excitation purity for average of s- and p-polarized, s- and p-polarized light. The data were calculated from scattering spectra.

Average of s- and p-polarized light				
Colour	x value	y value	Dominant wavelength (nm)	Excitation purity (%)
Cyan	0.18	0.10	455.0	79.4
Black	0.28	0.31	476.0	16.7
s-polarized light				
Colour	x value	y value	Dominant wavelength (nm)	Excitation purity (%)
Cyan	0.18	0.10	456	80.5
Black	0.28	0.31	476.5	17.1
p-polarized light				
Colour	x value	y value	Dominant wavelength (nm)	Excitation purity (%)
Cyan	0.19	0.12	455.5	74.6
Black	0.28	0.31	475	15.3

3.1.3 Discussion

In **Paper I** the complex refractive index of dry cyan and black inks was measured. The dominant wavelength and excitation purity of the inks were calculated from the spectrum of scattered light. When total internal reflectance measurements are used in colour determination, extra care should be used when interpreting the measurements due to the different results for s- and p-polarized light. The main difference in the colour of s- and p-polarized light is the excitation purity. In the ink development the colour difference of the s- and p-polarized light have some significance, but at the end product there is no effect on the visual appearance due to the unpolarized light.

3.2 BIOFUEL

The bio based fuels are one of the key technologies to provide an environmentally friendly way to transport people and goods [62, 63]. For fossil fuels, the quality is well controlled due to the mature level of the technology, but quality control of biofuels is not fully developed. A spectroscopic measurement is a convenient way to determine absorbing or scattering foreign matter in biofuels, however a problem arises if the unwanted substances are non-scattering and non-absorbing.

3.2.1 Samples

The samples used in **Paper II** were biologically and chemically treated Chilean Lenga tree and wheat samples in an ethanol matrix. The full description of the sample treatment can be found in **Paper II**. The amount of the dry sample comparing with the volume of ethanol was negligible, hence samples were not scattering.

3.2.2 Refractive index ratio in general case

In **Paper II** we presented how the refractive index ratio can be obtained from transmissions measurements. The assumption for obtaining the refractive index ratio from transmission spectra is that the sample is non-absorbing. If the assumption is fulfilled then detected light attenuation comes from cuvette-sample interface reflectance, which is governed by the Fresnel coefficients described in section 2.2.2. If the sample is less reflecting and absorbing than the reference then the measured transmittance increases and *vice versa*. A special case occurs if the sample is less reflecting and it has a higher absorption than the reference, this produces 100% transmittance but the sample can differ from the reference. The equation used in **Paper II** describing the absorbance difference is written as follows:

$$\Delta\alpha d = (\alpha_r - \alpha_s)d, \tag{3.1}$$

where α_r is the absorption coefficient of the reference, α_s is the absorption coefficient of the sample and d is the thickness of the sample. The absorption coefficients in Eq. (3.1) can be divided in to two parts: $\alpha = \alpha_A + \alpha_R/d$, where subscript A denotes the measured absorption coefficient due to the real absorption and subscript R denotes the measured absorption coefficient due to the reflection. The equation for $\Delta\alpha$ in terms of the real absorption and the detected absorption due to the reflection is written as follows:

$$\Delta\alpha d = ((\alpha_{rA} + \alpha_{rR}/d) - (\alpha_{sA} + \alpha_{sR}/d))d \tag{3.2}$$

An example of the behaviour of the measured refractive index ratio in the general case, where the assumption of non-absorbing reference and sample are not fulfilled, is shown in the Fig. 3.2. In the example the following refractive indexes are used: 1.46 for the cuvette, from 1 to 2 for the sample and 1.79 (or 1.19) for the reference, producing the measured absorbance of 0.01 due to the reflection. In the calculation a single interface was taken into account.

In the Fig. 3.2 the curved line indicates the measured unity of the refractive index ratio and the horizontal line is zero absorption difference in the frame of the real absorption. In Fig. 3.2 the vertical line is the zero reflection, where the sample and the cuvette have a perfect refractive index match. The red circles mark the intersections of the zero absorption difference line and measured refractive index unity curve. These intersections correspond to the perfect match between the sample and the reference. The two points where the sample and the reference produce a similar transmittance response, a rise from the square power form of the equations (2.22) and (2.24). From the measurement perspective, two correct values indicate that it is impossible to obtain the refractive index ratio of the sample and the reference without earlier knowledge of the refractive indices of the sample, cuvette, and reference. However, in real measurements the refractive indices of the cuvette and reference are known.

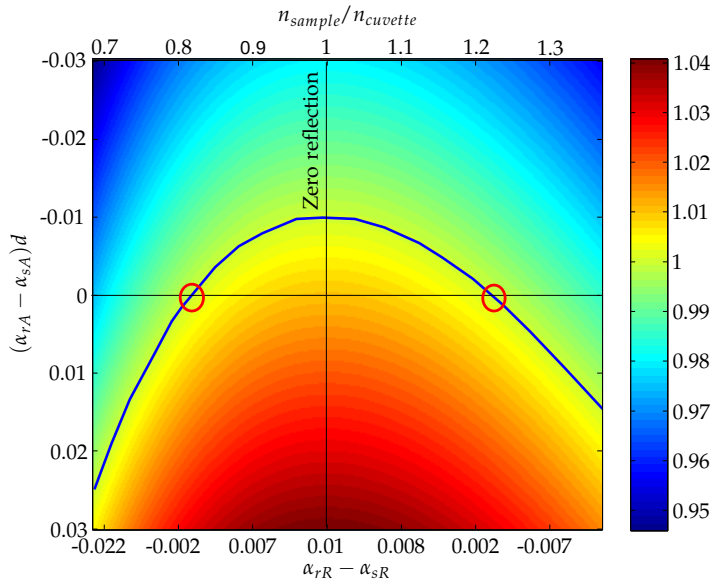

Figure 3.2: Measured and calculated refractive index ratio as a function of the measured absorbance difference between the sample and the reference. The y-axis is the absorbance difference due to the real absorption and the x-axis is the absorbance difference due to the surface reflections. In the x-axis on top of the figure is the refractive index ratio of the sample and cuvette.

3.2.3 Refractive index ratio of samples

In the measurements of **Paper II** the fused silica cuvettes refractive index was 1.45 at the wavelength 740 nm, which is in the middle of the studied spectral range, and the reference was ethanol with refractive index 1.36, which was also used to dilute the solid biosamples. The refractive index ratio of the samples was higher than unity almost in every sample. The average of the refractive index ratio from 680nm - 815nm is shown in Table 3.2.

Values larger than unity indicate that the samples have higher transmittance than the reference, hence samples are less reflecting than the reference. The decrease in the sample's reflectance is due to refractive index that is closer to the cuvette than to the reference. The increase of the samples refractive index can be caused

Table 3.2: Refractive index ratio data n_s/n_r of Lenga and Wheat samples from the spectral range of 680 - 815 nm.

	Lenga		Wheat	
Sample	Average	Std	Average	Std
1	1.0021	0.0001	1.0016	0.0002
2	1.0005	0.0001	1.0009	0.0001
3	1.0015	0.0002	0.9997	0.0001
4	1.0011	0.0002	1.0003	0.0001
5	1.0015	0.0001	1.0010	0.0001
6	1.0008	0.0001	1.0034	0.0001
7	1.0021	0.0001	0.9998	0.0001
8	1.0019	0.0003	1.0019	0.0001
9	1.0016	0.0002	1.0022	0.0002
10	1.0016	0.0003	1.0021	0.0001
11	1.0023	0.0003	1.0024	0.0001
12	1.0050	0.0003	1.0012	0.0000
13	1.0032	0.0000	1.0006	0.0001
14	1.0025	0.0001	1.0008	0.0001
15	1.0021	0.0001	1.0005	0.0001
16	1.0004	0.0001		

by different sugars for which the refractive indices are higher than that of ethanol. Refractive index ratio values lower than unity indicates that the samples reflectance is higher than the reference. The source of higher reflectance can be water contamination in the sample. The refractive index of water is 1.33 at the wavelength 740 nm, hence higher amounts of water increase the reflectance. Another explanation for values lower than unity is that the assumption that the sample is non-absorbing is not fulfilled and the transmittance difference is due to the real absorption.

3.2.4 Discussion

In **Paper II** the transmission spectra of the biofuel samples were measured and the method of obtaining the refractive index ratio of the sample and the reference was introduced. Without *prior* knowledge of the refractive indices of the sample, reference and cuvette the interpretation of the transmission spectra will provide ambiguous results. However, in practical measurements previous

knowledge of references and cuvettes provides enough information, in general, to discard incorrect results. The refractive index ratio method can be used to provide information from the sample in addition to traditional spectral analysis methods. The method has a great potential to be exploited in plants where bioethanol is produced.

3.3 GOLD COLLOID

Metallic nanoparticles (NP) are in the center of research due to their promising properties in areas like medicine [64–66], optics [67–69] and chemistry [70–72]. One focus in the research is the measurement of the NPs optical properties. The optical properties play a crucial role in the field of optics and in the detection and control of the NPs in the human body and in the environment [73–75]. In general, the studies are carried out using spectroscopy and the NPs are located in a liquid host, forming a colloid.

3.3.1 Gold colloid sample

The gold colloid sample used in **Papers III** and **IV** was purchased from Nanocs Inc. (NY, USA). The company provided information about the number density of gold NPs (7×10^{11} particles/ml). The gold NPs had an average diameter of 20 nm and a spherical shape. The NPs host liquid was water.

3.3.2 Permittivity of gold NP

In **Paper III** the complex permittivity of the NPs was obtained. The real part of the complex refractive index of the gold colloid was measured with a home-built reflectometer (REM) [76]. The gold colloid's imaginary part of the complex refractive index was obtained from transmission spectra and with the aid of equations (2.28) and (2.30). The NPs were in water solution and the real part of the complex refractive index was estimated using Partington's formula [77] and the imaginary part of the complex refractive index of water was estimated to be negligible. The above mentioned data was used in the Maxwell-Garnet model (2.11) and the complex permittivity of the gold NP was obtained. The validity of the results can be estimated by calculating the theoretical extinction spectra with the aid of the Mie theory using the complex permittivity of the NP obtained from the measurements and utilization of the MG model.

The equation used in Mie theory is written as follows [78,79]:

$$\alpha = \frac{18\pi N_s V n_{water}^3 \epsilon_{im}/\lambda}{(\epsilon_{real} + 2n_{water}^2)^2 + \epsilon_{im}^2}, \tag{3.3}$$

where N_s is the number density of the NPs, V is the volume of the NP, n_{water} is the refractive index of water obtained from Partington's formula, ϵ_{im} is the imaginary part of the permittivity of the NP, ϵ_{real} is the real part of the permittivity of the NP and λ is the wavelength. The measured and calculated extinction spectra of the gold colloid (100%, non-diluted) is shown in the Fig. 3.3. The calculated values correspond very closely to the measurement results, the difference spectrum of measured and calculated results is shown in Fig. 3.4.

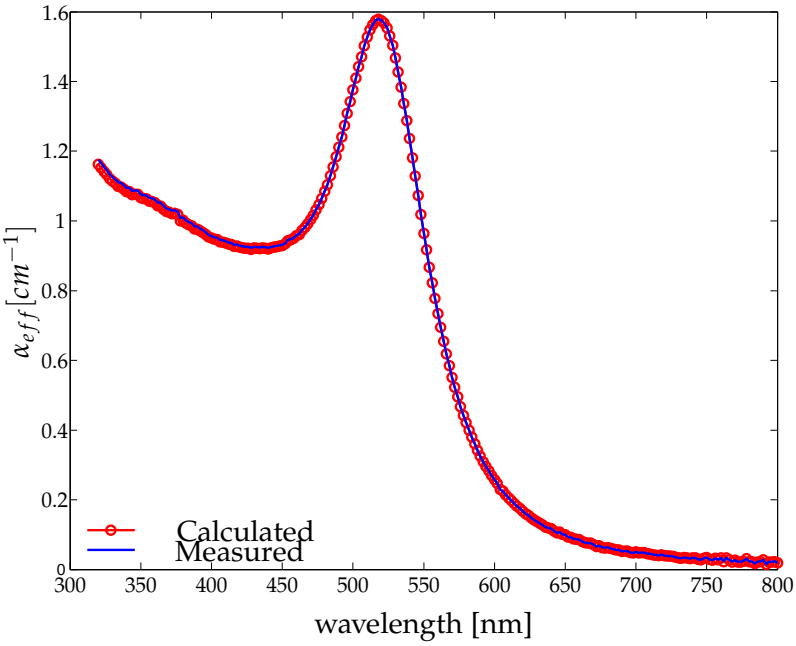

Figure 3.3: Measured and calculated effective absorption spectrum of non-diluted gold colloid.

In Fig. 3.4 the difference of the measured and calculated spectrum is increasing from 500nm to 300nm. One explanation of the low error is that the assumption of negligible absorption of water is not fulfilled in that region.

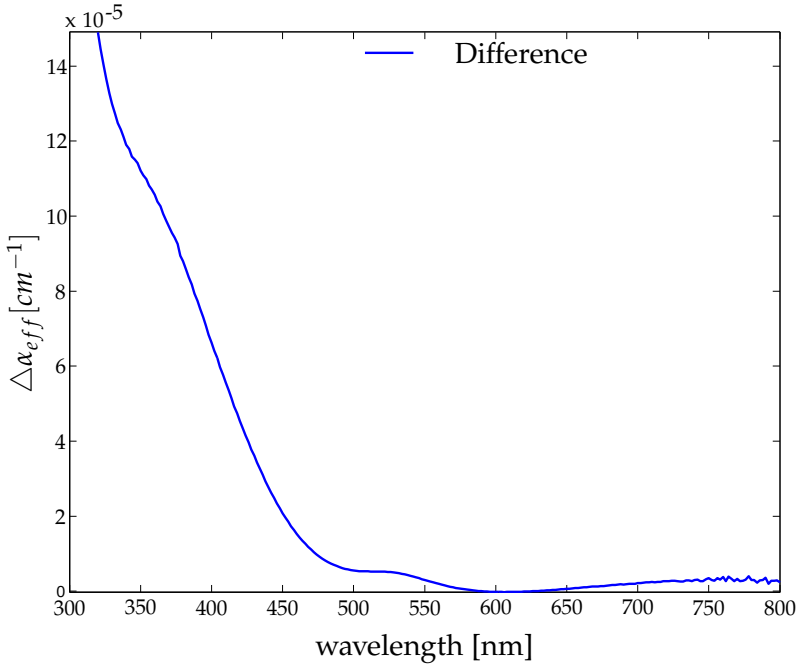

Figure 3.4: Difference of the measured and the calculated effective absorption spectrum of 100 % gold colloid.

3.3.3 Complex refractive index of gold colloid

In **Paper IV** the same commercial gold colloid samples were used as in **Paper III**. The dispersion of the refractive index of different dilutions of the gold colloid was obtained from the transmission spectra and with the aid of the Kramers–Kronig (KK) equation (2.18). The complex refractive index was also obtained for 100% gold colloid with the aid of the transmission spectroscopy and singly substractive Kramers–Kronig (SSKK) equation (2.20). The anchor point for the SSKK was measured with a commercial Abbe refractometer. The real and imaginary parts of the complex refractive index of the 100 % gold colloid are shown in Fig. 3.5.

In the Fig. 3.5 the absorption due to the SPR is clearly observed near the wavelength of 520 nm. A rapid drop of the real part of the complex refractive index near 300 nm is not a real property of the gold colloid, it is due to error in numerical evaluation of the SSKK.

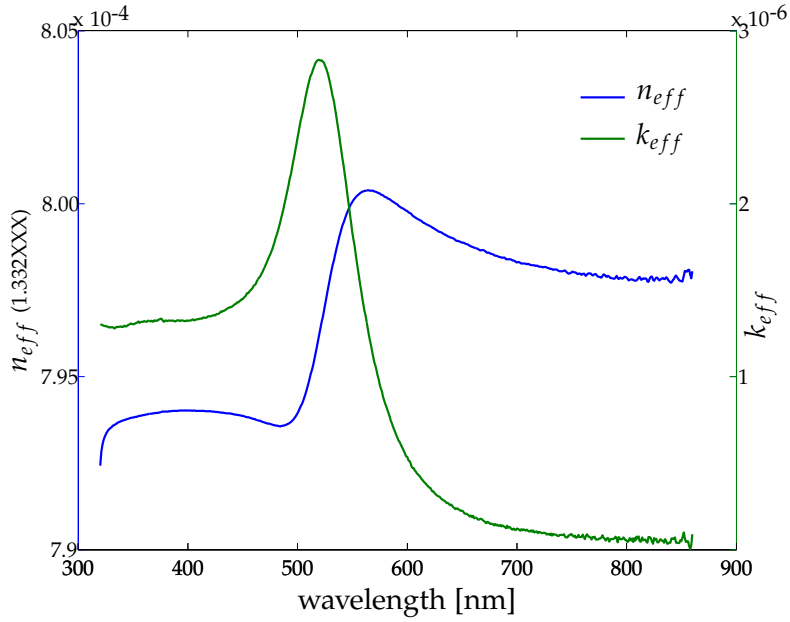

Figure 3.5: Real and imaginary part of the refractive index of 100 % gold colloid.

The error is inevitable because the measurement range is limited and values outside the measurement range must be extrapolated.

3.3.4 Number density of NPs

The normalized number density of NPs was calculated in **Paper III** using Smakula's formula. The number of the absorbing units in the gold colloid was 6800 times higher than the number of NPs in the sample. The number of gold atoms in the NP is several thousands, hence the number of absorbing units is reasonable. In **Paper IV** the number density of dispersion electrons in the sample was calculated with the f-sum rule. Both Smakula's formula and the f-sum rule produce results with a linear relationship with the dilution ratio and hence the same number of the NPs. The normalized number density of NPs calculated with Smakula's formula and with the f-sum rule are presented in Fig. 3.6.

As can be seen from Fig. 3.6 the f-sum rule and Smakula's for-

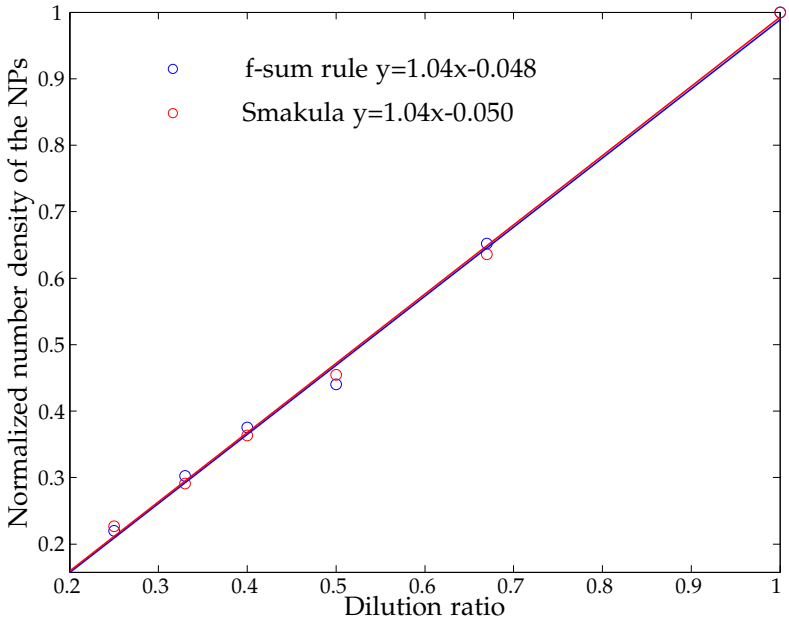

Figure 3.6: Normalized number density of NPs calculated with f-sum rule and Smakulas formula. Error is estimated to 5 % due to inaccuracy in dilution.

mula produce quite similar results. The reason for this is that basically both are measuring the same quantity. The difference is that the f-sum rule is an integral form and Smakula's formula utilizes the concepts of the full width at half maximum (FWHM). Also, the absorption peak of the SPR is close to a Lorentzian shape so the assumption of a Lorentzian line shape is fulfilled. If the absorption peak is not Gaussian or Lorentzian, the f-sum rule would produce a better result. For well behaving absorption peaks, the Smakula's formula is an easier choice due to the minimum amount of calculations.

3.3.5 Discussion

The complex permittivity of gold NP was obtained in **Paper III**. The obtained permittivity of the NP produces almost identical absorption spectra according to the Mie theory, hence the method is

accurate to describe the complex permittivity of NPs. Assumptions for the method are, the sample should be diluted and the extinction coefficient of the host liquid in the measurement range should be negligible.

In **Paper IV** the complex refractive index of the gold colloid was obtained with the aid of transmission spectroscopy, KK and SSKK analysis. The shape of the dispersion curve is very similar as in the article [80] where small silver NPs were embedded in the glass host. The similar shape of the dispersion curves originates from NPs in both samples (in **Paper IV** and [80]). In both cases the measured absorption is due to the SPR, which produces a similar peak, but in a different position of the spectrum.

The normalized number density of NPs was measured in **Paper III** and the number density of dispersion electrons was measured in **Paper IV**. In **Paper III** Smakula's formula was used and in **Paper IV** the f-sum rule was utilized. Both produce a linear relationship with the dilution relationship and there are no big differences between the results. The f-sum rule is a more general method for obtaining the amount of the NPs in the sample, however Smakula's formula is easier to use at least if the studied absorption peak fits either a Gaussian or Lorentzian lineshape.

3.4 TURBIDITY AND FORMAZINE

Turbidity is the haziness or cloudiness of a liquid caused by small particles which scatter light. The measurement of the turbidity is standardized for example by the International Organization for Standardization (ISO) [81], American Society for Testing and Materials (ASTM) [82] and the United States Environmental Protection Agency (USEPA) [83]. In the standards, the scattered light is measured at 90° relative to the incoming light, and the amount of scattered light is compared with the measurement result from the formazine standard. However, standard methods do not necessarily produce accurate results due to the complex nature of the sample and scattering phenomena. To overcome the complexity problem it

Table 3.3: Properties of water matrices and their expected effect on turbidity measurement [84]

Properties of water matrix	**Effect on the measurement**	**Direction of effect on the measurement**	**Instrument designs to compensate for effect**
Colored particles	Absorption of light beam	Negative	Near IR (780-900 nm) light source Multiple detectors
Colour, dissolved (in the matrix)	Absorption of light beam (if the incident light wavelengths overlap the absorptive spectra within the sample matrix)	Negative	Near IR (780-900 nm) light source Multiple detectors
Particle size:	*Wavelength dependent.*		
Large particles	Scatter long wavelengths of light more readily than small particles	Positive (for near IR light source, 820-900 nm)	White light (broad spectrum) light source
Small particles	Scatter short wavelengths of light more efficiently than long wavelengths	Positive (for broad spectrum light source, such as white light)	Near IR (780-900 nm) light source
Particle Density	Increases forward and backward scattering of light at high densities	Negative	Multiple detectors Backscattering

is possible to use different measurement geometries, multiple detectors and different measurement wavelengths to get a better picture from the sample. Some effects on measurement result and compensation methods for the water host sample are shown in the Table 3.3.

Formazine is a standard reference for turbidity measurements and it is used to estimate the turbidity of unknown samples. Formazine ($C_2H_4N_2$) standard is made by mixing 5 g/l hydrazine sulfate ($H_6N_2O_4S$) and 50 g/l hexamethylenetetramine ($C_6H_{12}N_4$). The above-mentioned ratio produces a formazine sample with the turbidity of 4000 FTU. To produce samples with a lower turbidity, the original sample should be diluted with ultra pure water.

3.4.1 Samples

The formazine sample of 4000 FTU used in **Paper V** was purchased from Hach LANGE Gmbh (Düsseldorf,Germany). The formazine sample was used to produce turbidities 1 (clear water) to 800 FTU. Blue food-colouring dye was used to produce an absorbing host liquid. Different absorbing levels of host liquid were obtained using 0.02, 0.04, and 0.06 ml of food-colouring dye.

3.4.2 Measurement results

In **Paper V**, we demonstrated the measurement setup to minimize the effect of colored host liquid on the turbidity reading, utilizing evanscent field scattering from particles in the liquid. The standard deviation of dynamic speckle [85, 86] was found to correlate well with the turbidity of the sample. In Table 3.3 it is proposed to use a near IR light source to overcome the absorbance problem of the host liquid. However, in the general case it does not work, because the host liquid can absorb in the chosen spectral range. As can be seen from Fig. 3.7 the absorbance from the host liquid has some effect on the turbidity reading. The maximum error of standard deviation of dynamic speckle between colourless and the dye colored host liquid was 2.2 %, 2.2 % and 3.6 %.

From Fig. 3.7 it can be seen also that the relationship between the dynamic speckle and the turbidity value is not linear. The non-linear relationship indicates that for high turbidity values the dynamic speckle underestimates the real turbidity of the sample and eventually becomes insensitive to turbidity changes. The first derivatives of the fitting curves are shown in Fig. 3.8. From Fig. 3.8 it can be seen that near 800 FTU the change of dynamic speckle as a function of turbidity is near zero and hence the system is insensitive to the change of turbidity in higher levels.

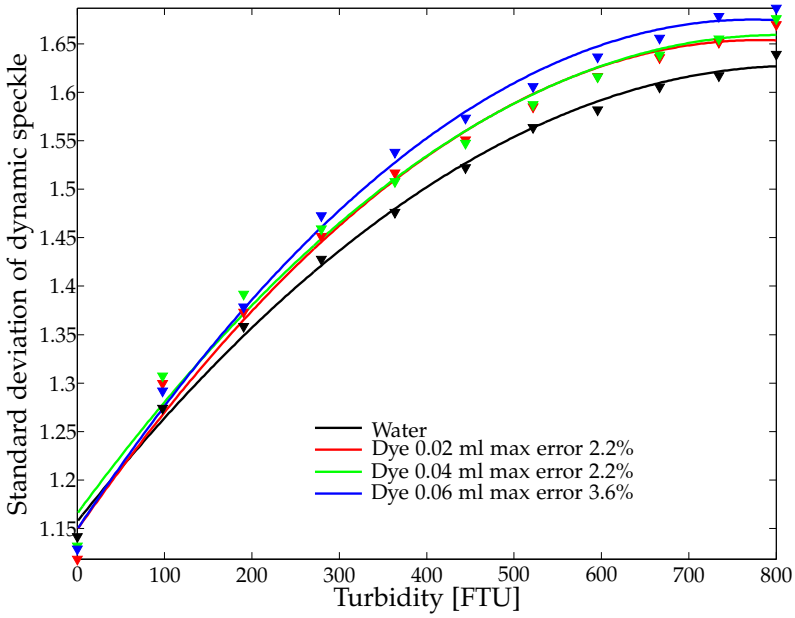

Figure 3.7: Standard deviation of dynamic speckle as a function of turbidity for clear and colored samples.

3.4.3 Discussion

In **Paper V** the evanescent field scattering from colored- and water-formazine samples was measured. The standard deviation of dynamic speckle was found to be in good correlation with the turbidity of formazine samples. The setup has some sensitivity to the colour of the host liquid. The upper limit of the dynamic range of measurement was found to be 800 FTU with the current measurement geometry.

3.5 SUMMARY AND OUTLOOK

The MFS in **Paper I** is reliable and an accurate way to measure the optical properties of a liquid and it can be used with success in the future. In the future, research on the complex refractive index of formazine, especially how it will change change over time, would

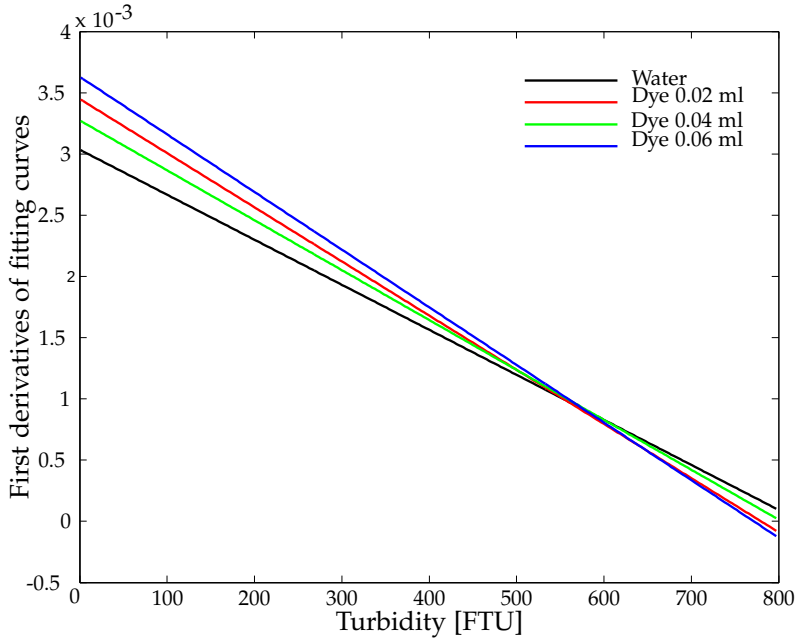

Figure 3.8: The first derivatives of the fitting functions of the measured standard deviation of the dynamic speckle from clear and colored samples.

be interesting.

Refractive index ratio measurement with the aid of the transmission spectra proposed in **Paper II** is not fully developed. The drawback of the proposed method, in the general case, is the ambiguous results obtained, and more work needs to be done to overcome this issue. Another challenge is to find a way to be sure that in the studied spectral range, absorption is not taking place, and that the assumption for the non-absorbing sample is fulfilled. If these issues can be solved then the method can be used to obtain the refractive index n, at least, in some part of the spectral range. The obtained refractive index can be used in the SSKK as the anchor point. The combination can give a good picture of the sample in terms of n and k in a relatively large spectral range. The benefit of using the spectrophotometer is not that it gives the most accurate measurement of the refractive index, but to provide a new way

to utilize an instrument that is used in a wide variety of different industrial fields.

The usage of the f-sum rule and Smakula's formula are well known and they can be used to estimate the number density of the NPs in the liquid, as was presented in **Papers III** and **IV**. Also, the KK and the SSKK analysis are convenient ways to get the optical properties of the colloids. The utilization of the MG model and the measured refractive index and extinction of gold colloid provides good results compared with the Mie's theory. The final test for the method would be to obtain similar NPs in two different host liquids and measure optical properties of the NPs, as described in **Paper III**. The measured optical properties of NPs should be used to calculate the absorbance spectra of the sample, with different host liquids. The procedure would give an estimate for the effect of host liquid on the measured optical properties of the NPs.

The measurement setup in **Paper V** was used to measure the turbidity of a liquid using a dynamic speckle. In the future, one interesting study would be the temporal evolution of a static speckle. The study of a static part of the speckle may provide information of the fouling of the measurement prism. Also, how the different setup geometries affect the sensitivity and dynamic of the measurements should be studied.

4 Conclusions

New methods of obtaining the optical properties of complex liquids have been presented in this thesis. The methods can be divided in to two groups. The first group consists of data analysis and measurement techniques that can be executed with existing instruments (**Papers I-IV**). The second group includes a novel measurement technique to study complex liquids (**Paper V**).

The complex refractive indices and colours of black and cyan inks were obtained with MFS in **Paper I**. The method can be treated as a fully developed method and can be used in the future. The colour of the inks varies slightly, depending on which polarization is used in the calculations. If the method is used in the future in colour measurements, extra attention should be paid to the interpretation of the results.

In **Paper II** a method to estimate a refractive index ratio of a biofuel sample was presented. The method is not fully developed and needs more research to be evolved into a fully functional practical method of measurement. In a general case results will be ambiguous and advance knowledge from the sample, cuvettes and reference must be obtained.

The complex permittivity of spherical gold NPs was obtained in **Paper III**. The complex permittivity obtained produces good results when used in Mie's theory. The method is very promising in obtaining optical properties of spherical NPs.

The number density of NPs from colloidal gold was obtained in **Papers III** and **IV** with the aid of Smakula's formula and f-sum rule. Both methods produce similar results, due to the well behaved absorption peak of the SPR. In **Paper IV** the complex refractive index of colloidal gold was obtained with the transmission spectra and using KK and SSKK analysis. The results are in line with previous results and the method can be used with success to obtain the optical properties of colloidal NPs.

Turbidity of the dyed formazine samples was measured with the new measurement setup in **Paper V**. The measurement is based on evanescent field scattering from solid particles in a host liquid. The scattered field produces a dynamic speckle pattern to CCD camera. The standard deviation of the dynamic speckle correlates with the turbidity of a formazine sample. The results have some dependency on the absorbance due to the dyed host liquid.

Bibliography

[1] M. Juuti, H. Tuononen, T. Prykäri, V. Kontturi, M. Kuosmanen, E. Alarousu, J. Ketolainen, R. Myllylä, and K. Peiponen, "Optical and terahertz measurement techniques for flat-faced pharmaceutical tablets: a case study of gloss, surface roughness and bulk properties of starch acetate tablets," *Meas. Sci. Technol.* **20,** 015301 (2009).

[2] A. Lehmuskero, V. Kontturi, J. Hiltunen, and M. Kuittinen, "Modeling of laser-colored stainless steel surfaces by color pixels," *Appl. Phys. B* **98,** 497–500 (2009).

[3] P. Silfsten, V. Kontturi, T. Ervasti, J. Ketolainen, and K. Peiponen, "Kramers-Kronig analysis on the real refractive index of porous media in the terahertz spectral range," *Opt. Lett.* **36,** 778–780 (2011).

[4] M. O. A Mäkinen, V. Kontturi, T. Jääskeläinen, and J. Parkkinen, "Evaluation of Print-through with Colour Theory: Uniform and Nonuniform Prints," *J. Pulp Pap. Sci.* **34,** 161–168 (2008).

[5] W. R. M. Kenzie, N. J. Hoxie, M. E. Proctor, M. S. Gradus, K. A. Blair, D. E. Peterson, J. J. Kazmierczak, D. G. Addiss, K. R. Fox, and J. B. Rose, "A massive outbreak in Milwaukee of cryptosporidium infection transmitted through the public water supply," *N. Engl. J. Med.* **331,** 161–167 (1994), PMID: 7818640.

[6] C. J. Schuster, A. G. Ellis, W. J. Robertson, D. F. Charron, J. J. Aramini, B. J. Marshall, and D. T. Medeiros, "Infectious disease outbreaks related to drinking water in Canada, 1974-2001," *Can. J. Public Healt* **96,** 254–258 (2005), PMID: 16625790.

[7] J. Laine, E. Huovinen, M. J. Virtanen, M. Snellman, J. Lumio, P. Ruutu, E. Kujansuu, R. Vuento, T. Pitkänen, I. Miettinen, J. Herrala, O. Lepist, J. Antonen, J. Helenius, M. Hänninen, L. Maunula, J. Mustonen, M. Kuusi, and Pirkanmaa Waterborne Outbreak Study Group, "An extensive gastroenteritis outbreak after drinking-water contamination by sewage effluent, Finland," *Epidemiol. Infect.* **139,** 1105–1113 (2010).

[8] K. Yao, M. T. Habibian, and C. R. O'Melia, "Water and waste water filtration. Concepts and applications," *Environ. Sci. Technol.* **5,** 1105–1112 (1971).

[9] R. Nilsson, "Removal of metals by chemical treatment of municipal waste water," *Water Res.* **5,** 51–60 (1971).

[10] J. G. Dean, F. L. Bosqui, and K. H. Lanouette, "Removing heavy metals from waste water," *Environ. Sci. Technol.* **6,** 518–522 (1972).

[11] G. Thompson, J. Swain, M. Kay, and C. F. Forster, "The treatment of pulp and paper mill effluent: a review," *Bioresource Technol.* **77,** 275–286 (2001).

[12] L. Chapman, "Transport and climate change: a review," *J. Transport Geogr.* **15,** 354–367 (2007).

[13] G. Sivakumar, D. R. Vail, J. Xu, D. M. Burner, J. O. Lay, X. Ge, and P. J. Weathers, "Bioethanol and biodiesel: Alternative liquid fuels for future generations," *Eng. Life Sci.* **10,** 8–18 (2010).

[14] S. Jacobs, G. Gould, and P. Rabinowitz, "Coherent Light Amplification in Optically Pumped Cs Vapor," *Phys. Rev. Lett.* **7,** 415–417 (1961).

[15] T. H. Maiman, "Stimulated Optical Radiation in Ruby," *Nature* **187,** 493–494 (1960).

[16] Y. B. Band, *Light and Matter*, 1st ed. (Wiley, New York, 2006).

[17] A. L. Schawlow and C. H. Townes, "Infrared and Optical Masers," *Phys. Rev.* **112,** 1940–1949 (1958).

[18] W. Boyle and G. Smith, "Charge coupled semiconductor devices," *Bell System Tech. J* **49,** 587–593 (1970).

[19] P. G. Cielo, *Optical Techniques for Industrial Inspection* (Academic Press, 1988).

[20] J. A. Dittman, J. B. Shanley, C. T. Driscoll, G. R. Aiken, A. T. Chalmers, and J. E. Towse, "Ultraviolet absorbance as a proxy for total dissolved mercury in streams," *Environ. Pollut.* **157,** 1953–1956 (2009).

[21] L. Fang, S. Chen, D. Li, and H. Li, "Use of Reflectance Ratios as a Proxy for Coastal Water Constituent Monitoring in the Pearl River Estuary," *Sensors* **9,** 656–673 (2009).

[22] A. M. Zysk, F. T. Nguyen, A. L. Oldenburg, D. L. Marks, and S. A. Boppart, "Optical coherence tomography: a review of clinical development from bench to bedside," *J. Biomed. Opt.* **12,** 051403 (2007).

[23] D. R. Leff, O. J. Warren, L. C. Enfield, A. Gibson, T. Athanasiou, D. K. Patten, J. Hebden, G. Z. Yang, and A. Darzi, "Diffuse optical imaging of the healthy and diseased breast: A systematic review," *Breast Cancer Res. Tr.* **108,** 9–22 (2007).

[24] A. Amelink, J. Haringsma, and H. J. Sterenborg, "Noninvasive measurement of oxygen saturation of the microvascular blood in Barrett's dysplasia by use of optical spectroscopy," *Gastrointest. Endosc.* **70,** 1–6 (2009).

[25] F. Wooten, *Optical properties of solids.* (Academic Press, New York, 1972).

[26] I. Kenyon, *The light fantastic : a modern introduction to classical and quantum optics* (Oxford University Press, Oxford, 2008).

[27] E. Hecht, *Optics*, 4th ed. (Addison-Wesley, Reading Mass., 2002).

[28] L. B. Scaffardi and J. O. Tocho, "Size dependence of refractive index of gold nanoparticles," *Nanotechnology* **17,** 1309–1315 (2006).

[29] H. Inouye, K. Tanaka, I. Tanahashi, and K. Hirao, "Ultrafast dynamics of nonequilibrium electrons in a gold nanoparticle system," *Phys. Rev. B: Condens. Matter* **57,** 11334–11340 (1998).

[30] C. Granqvist and O. Hunderi, "Optical properties of ultrafine gold particles," *Phys. Rev. B: Condens. Matter* **16,** 3513–3534 (1977).

[31] U. Kreibig, "Electronic properties of small silver particles: the optical constants and their temperature dependence," *J. Phys. F: Met. Phys* **4,** 999–1014 (1974).

[32] U. Kreibig and C. v. Fragstein, "The limitation of electron mean free path in small silver particles," *Z. Phys. A: Hadrons Nucl.* **224,** 307–323 (1969).

[33] U. Kreibig and L. Genzel, "Optical absorption of small metallic particles," *Surf. Sci.* **156,** 678–700 (1985).

[34] H. Hövel, S. Fritz, A. Hilger, U. Kreibig, and M. Vollmer, "Width of cluster plasmon resonances: Bulk dielectric functions and chemical interface damping," *Phys. Rev. B: Condens. Matter* **48,** 18178–18188 (1993).

[35] C. Bohren and D. Huffman, *Absorption and scattering of light by small particles* (Wiley, New York, 1983).

[36] S. Underwood and P. Mulvaney, "Effect of the Solution Refractive Index on the Color of Gold Colloids," *Langmuir* **10,** 3427–3430 (1994).

[37] J. C. M. Garnett, "Colours in Metal Glasses, in Metallic Films, and in Metallic Solutions. II," *Philos. Trans. R. Soc. London, Ser. A* **205,** 237–288 (1906).

[38] R. Ruppin, "Evaluation of extended Maxwell-Garnett theories," *Opt. Commun.* **182,** 273–279 (2000).

[39] W. Doyle, "Optical properties of a suspension of metal spheres," *Phys. Rev. B* **39,** 9852–9858 (1989).

[40] L. Landau, E. Lifshitz, and L. Pitaevski, *Electrodynamics of continuous media*, 2nd ed. (Pergamon press, Oxford, 1984).

[41] H. A. Kramers, "La deffusion de la lumiere par les atomes," *Atti del Congresso Internazionale dei Fisici* **12,** 545–557 (1926).

[42] R. D. L. Kronig, "On the theory of dispersion of x-rays," *J. Opt. Soc. Am.* **12,** 547–556 (1926).

[43] J. Räty, K. Peiponen, and T. Asakura, *UV-visible reflection spectroscopy of liquids* (Springer, Berlin, 2004).

[44] J. Toll, "Causality and the Dispersion Relation: Logical Foundations," *Phys. Rev* **104,** 1760–1770 (1956).

[45] H. Nussenzveig, *Causality and dispersion relations* (Academic Press, New York, 1972).

[46] R. K. Ahrenkiel, "Modified Kramers-Kronig Analysis of Optical Spectra," *J. Opt. Soc. Am* **61,** 1651–1655 (1971).

[47] F. Mirabella, *Internal reflection spectroscopy : theory and applications* (Marcel Dekker, New York, 1993).

[48] J. G. Sole, *An introduction to the optical spectroscopy of inorganic solids* (J. Wiley, Hoboken NJ, 2005).

[49] D. Y. Smith, Chap "Dispersion Theory, Sum Rules, and Their Application to Analysis of Optical Data" in *Handbook of optical constants of solids* (Academic Press, 1985).

[50] D. Smith and D. Dexter, "V Optical Absorption Strengths of Defects in Insulators The f-Sum Rule, Smakula's Equation, Effective Fields, and Application to Color Centers in Alkali Halides," in *Progress in Optics*, Vol. 10 (Elsevier, 1972), pp. 165–228.

[51] A. Smakula, "Über Erregung und Entfärbung lichtelektrisch leitender Alkalihalogenide," *Z. Phys. A: Hadrons Nucl.* **59,** 603–614 (1930).

[52] W. Doyle, "Optical Absorption by F Centers in Alkali Halides," *Phys. Rev.* **111,** 1072–1077 (1958).

[53] W. D. Wright, "A re-determination of the trichromatic coefficients of the spectral colours," *Trans. Opt. Soc.* **30,** 141–164 (1929).

[54] J. Guild, "The Colorimetric Properties of the Spectrum," *Philos. Trans. R. Soc. London, Ser. A* **230,** 149–187 (1932).

[55] W. S. Stiles and J. M. Burch, "N.P.L. Colour-matching Investigation: Final Report (1958)," *J. Mod. Opt.* **6,** 1–26 (1959).

[56] N. I. Speranskaya, "Determination of spectrum color coordinates for twenty-seven normal observers," *OPT SPECTROSC+* **7,** 424–428 (1959).

[57] G. Wyszecki, *Color Science : concepts and methods, quantitative data and formulae.*, 2nd ed. (Wiley, New York, 2000).

[58] Comission Internationale de l'Eclairage, "Selected colorimetric tables," `http://www.cie.co.at/index.php/LEFTMENUE/DOWNLOADS` (valid 27.5.2011).

[59] N. Pauler, *Paper optics* (AB Lorentzen & Wettre, Kista Sweden, 2000).

[60] H. Kipphan, *Handbook of print media : technologies and production methods* (Springer, Berlin, 2001).

[61] I. Niskanen, J. Räty, and K. Peiponen, "A multifunction spectrophotometer for measurement of optical properties of transparent and turbid liquids," *Meas. Sci. Technol.* **17,** N87–N91 (2006).

[62] P. S. Nigam and A. Singh, "Production of liquid biofuels from renewable resources," *Prog. Energy Combust. Sci.* **37,** 52–68 (2011).

[63] A. J. Ragauskas, C. K. Williams, B. H. Davison, G. Britovsek, J. Cairney, C. A. Eckert, W. J. Frederick, J. P. Hallett, D. J. Leak, C. L. Liotta, J. R. Mielenz, R. Murphy, R. Templer, and T. Tschaplinski, "The Path Forward for Biofuels and Biomaterials," *Science* **311,** 484–489 (2006).

[64] D. Pissuwan, S. M. Valenzuela, and M. B. Cortie, "Therapeutic possibilities of plasmonically heated gold nanoparticles," *Trends Biotechnol.* **24,** 62–67 (2006).

[65] N. Sanvicens and M. P. Marco, "Multifunctional nanoparticles - properties and prospects for their use in human medicine," *Trends Biotechnol.* **26,** 425–433 (2008).

[66] A. R. Shahverdi, A. Fakhimi, H. R. Shahverdi, and S. Minaian, "Synthesis and effect of silver nanoparticles on the antibacterial activity of different antibiotics against Staphylococcus aureus and Escherichia coli," *Nanomed. Nanotechnol. Biol. Med.* **3,** 168–171 (2007).

[67] J. Butet, J. Duboisset, G. Bachelier, I. Russier-Antoine, E. Benichou, C. Jonin, and P. Brevet, "Optical Second Harmonic Generation of Single Metallic Nanoparticles Embedded in a Homogeneous Medium," *Nano Lett.* **10,** 1717–1721 (2010).

[68] D. M. Schaadt, B. Feng, and E. T. Yu, "Enhanced semiconductor optical absorption via surface plasmon excitation in metal nanoparticles," *Appl. Phys. Lett.* **86,** 063106 (2005).

[69] M. Danckwerts and L. Novotny, "Optical Frequency Mixing at Coupled Gold Nanoparticles," *Phys. Rev. Lett.* **98,** 026104 (2007).

[70] M. Chen and D. W. Goodman, "Catalytically Active Gold: From Nanoparticles to Ultrathin Films," *Acc. Chem. Res.* **39,** 739–746 (2006).

[71] V. P. Ananikov, N. V. Orlov, I. P. Beletskaya, V. N. Khrustalev, M. Y. Antipin, and T. V. Timofeeva, "New Approach for Size- and Shape-Controlled Preparation of Pd Nanoparticles with Organic Ligands. Synthesis and Application in Catalysis," *J. Am. Chem. Soc.* **129,** 7252–7253 (2007).

[72] M. A. Albrecht, C. W. Evans, and C. L. Raston, "Green chemistry and the health implications of nanoparticles," *Green Chem.* **8,** 417–432 (2006).

[73] F. F. Larese, F. D'Agostin, M. Crosera, G. Adami, N. Renzi, M. Bovenzi, and G. Maina, "Human skin penetration of silver nanoparticles through intact and damaged skin," *Toxicology* **255,** 33–37 (2009), PMID: 18973786.

[74] R. D. Handy, F. Kammer, J. R. Lead, M. Hassellv, R. Owen, and M. Crane, "The ecotoxicology and chemistry of manufactured nanoparticles," *Ecotoxicology* **17,** 287–314 (2008).

[75] H. S. Sharma, S. Hussain, J. Schlager, S. F. Ali, and A. Sharma, "Influence of nanoparticles on blood-brain barrier permeability and brain edema formation in rats," *Acta Neurochir. Suppl.* **106,** 359–364 (2010), PMID: 19812977.

[76] J. Räty, E. Keränen, and K. Peiponen, "The complex refractive index measurement of liquids by a novel reflectometer apparatus for the UV - visible spectral range," *Meas. Sci. Technol.* **9,** 95–99 (1998).

[77] J. R. Partington, *An advanced treatise on physical chemistry: volume 4 Physico-chemical optics* (Longmans, 1960).

[78] R. Doremus, S. Kao, and R. Garcia, "Optical absorption of small copper particles and the optical properties of copper," *Appl. Opt.* **31,** 5773–5778 (1992).

[79] G. Mie, "Beiträge zur Optik trüber Medien, speziell kolloidaler Metallösungen," *Ann. Phys.* **330,** 377–445 (1908).

[80] U. Kreibig, "Kramers Kronig analysis of the optical properties of small silver particles," *Z. Phys. A: Hadrons Nucl.* **234,** 307–318 (1970).

[81] "ISO 7027, Water Quality-Determination of Turbidity," (1999).

[82] "ASTM D6855-03 Standard Test Method for Determination of Turbidity Below 5 NTU in Static Mode," (2003).

[83] "USEPA, Method 180.1, Determination of Turbidity by Nephelometry," (1993).

[84] C. W. Anderson, Chap A.6 Field Measurements Section 6.7 Turbidity in *U.S Geological Survey Techniques of Water-Resources Investigations* (U.S Geological Survey, 2005).

[85] J. W. Goodman, "Some fundamental properties of speckle," *J. Opt. Soc. Am.* **66,** 1145–1150 (1976).

[86] R. Erf, *Speckle metrology* (Academic Press, New York, 1978).

Ville Kontturi

Optical measurements of complex liquids

In this thesis novel methods of measuring optical properties of complex liquids are presented. The methods can be divided in to two groups, data analysis and sensor development. In the data analysis, data from common measurement devices is used in a novel way to obtain optical properties of the samples. In the sensor development approach a new measurement setup is introduced to measure the turbidity of the sample. The presented methods have possible applications in a different line of industry, healthcare and environment protection.

UNIVERSITY OF
EASTERN FINLAND

Publications of the University of Eastern Finland
Dissertations in Forestry and Natural Sciences

ISBN: 978-952-61-0587-1 (PDF)
ISSNL: 1798-5668
ISSN: 1798-5676